

RESEARCH ARTICLE

Influence of ionizable lipid tail length on lipid nanoparticle delivery of mRNA of varying length

Kaitlin Mrksich¹ | Marshall S. Padilla¹ | Ryann A. Joseph¹ | Emily L. Han¹ |
 Dongyoon Kim¹ | Rohan Palanki^{1,2} | Junchao Xu¹ | Michael J. Mitchell^{1,3,4,5,6,7,8} 

¹Department of Bioengineering, School of Engineering and Applied Science, University of Pennsylvania, Philadelphia, Pennsylvania, USA

²Center for Fetal Research, Children's Hospital of Philadelphia, Philadelphia, Pennsylvania, USA

³Abramson Cancer Center, Perelman School of Medicine, University of Pennsylvania, Philadelphia, Pennsylvania, USA

⁴Center for Cellular Immunotherapies, Perelman School of Medicine, University of Pennsylvania, Philadelphia, Pennsylvania, USA

⁵Penn Institute for RNA Innovation, Perelman School of Medicine, University of Pennsylvania, Philadelphia, Pennsylvania, USA

⁶Institute for Immunology, Perelman School of Medicine, University of Pennsylvania, Philadelphia, Pennsylvania, USA

⁷Cardiovascular Institute, Perelman School of Medicine, University of Pennsylvania, Philadelphia, Pennsylvania, USA

⁸Institute for Regenerative Medicine, Perelman School of Medicine, University of Pennsylvania, Philadelphia, Pennsylvania, USA

Correspondence

Michael J. Mitchell, Department of Bioengineering, School of Engineering and Applied Science, University of Pennsylvania, Pennsylvania, PA 19104, USA.
 Email: mjmittch@seas.upenn.edu

Funding information

National Institutes of Health, Grant/Award Number: DP2 TR002776; US National Institutes of Health (NIH) Director's New Innovator Award; Burroughs Wellcome Fund Career Award at the Scientific Interface (CASI); American Cancer Society, Grant/Award Number: RSG-22-122-01-ET; NSF CAREER Award, Grant/Award Number: CBET-2145491; National Institute of Dental & Craniofacial Research (NIDCR) of the NIH under Award Number, Grant/Award Number: T90DE030854; Center for Innovation & Precision Dentistry (CiPD) at the University of Pennsylvania; National Science Foundation (NSF) Graduate Research Fellowship, Grant/Award Number: 1845298; NIH NHLBI F30 fellowship, Grant/Award Number: F30HL162465-01A1; NSF Major Research Instrumentation Program, Grant/Award Number: NSF CHE-1827457; Vagelos Institute for Energy Science and Technology

Abstract

RNA-based therapeutics have gained traction for the prevention and treatment of a variety of diseases. However, their fragility and immunogenicity necessitate a drug carrier. Lipid nanoparticles (LNPs) have emerged as the predominant delivery vehicle for RNA therapeutics. An important component of LNPs is the ionizable lipid (IL), which is protonated in the acidic environment of the endosome, prompting cargo release into the cytosol. Currently, there is growing evidence that the structure of IL lipid tails significantly impacts the efficacy of LNP-mediated mRNA translation. Here, we optimized IL tail length for LNP-mediated delivery of three different mRNA cargos. Using C12-200, a gold standard IL, as a model, we designed a library of ILs with varying tail lengths and evaluated their potency in vivo. We demonstrated that small changes in lipophilicity can drastically increase or decrease mRNA translation. We identified that LNPs formulated with firefly luciferase mRNA (1929 base pairs) and C10-200, an IL with shorter tail lengths than C12-200, enhance liver transfection by over 10-fold. Furthermore, different IL tail lengths were found to be ideal for transfection of LNPs encapsulating mRNA cargos of varying sizes. LNPs formulated with erythropoietin (EPO), responsible for stimulating red blood cell production, mRNA (858 base pairs), and the C13-200 IL led to EPO translation at levels similar to the C12-200 LNP. The LNPs formulated with Cas9 mRNA (4521 base pairs) and the C9-200 IL induced over three times the quantity of indels compared with the C12-200 LNP. Our findings suggest that shorter IL tails may lead to higher transfection of LNPs encapsulating larger mRNAs, and that longer IL tails may be more efficacious for delivering smaller mRNA cargos. We envision that the results of this project

This is an open access article under the terms of the [Creative Commons Attribution](https://creativecommons.org/licenses/by/4.0/) License, which permits use, distribution and reproduction in any medium, provided the original work is properly cited.

© 2024 The Authors. *Journal of Biomedical Materials Research Part A* published by Wiley Periodicals LLC.

can be utilized as future design criteria for the next generation of LNP delivery systems for RNA therapeutics.

KEYWORDS

ionizable lipid, lipid nanoparticle, mRNA

1 | INTRODUCTION

Messenger RNA (mRNA) therapeutics have shown immense potential for a range of applications, including cancer immunotherapy,^{1–3} vaccine development,^{4–7} and gene editing.^{8–10} However, a significant barrier for the delivery of these therapeutics is their negative charge and large size, which prevents them from entering cells and leads to rapid degradation and immune recognition.¹¹ This has necessitated the use of nanoparticles as delivery vehicles.^{12–14} Lipid nanoparticles (LNPs) have emerged as the preeminent delivery vehicle for RNA therapies, most recently as the carriers for both the Moderna (Spikevax) and Pfizer/BioNTech (Comirnaty) mRNA COVID-19 vaccines.^{15–17}

LNPs consist of an ionizable lipid (IL), a phospholipid, cholesterol, and a PEGylated lipid, with the IL playing an essential role in intracellular RNA delivery.^{18,19} The ionizable nature of ILs allows for encapsulation of mRNA cargo into LNPs.^{20,21} Furthermore, the hydrophobic nature of ILs permits their integration into the lipid core of LNPs.^{22,23} Thus, ILs must strike a balance between ionizability and hydrophobicity for successful encapsulation of mRNA into LNPs. ILs are protonated in the endosome due to its acidic conditions, which prompts cargo release into the cytosol.²⁴ With endosomal escape being one of the most consequential barriers to RNA delivery, ILs serve an important role in facilitating this process.^{25–28} Organ tropisms of LNPs are also guided by ILs due to the formation of protein coronas,^{29–33} targeted delivery to specific cell types,^{34,35} and specific uptake pathways.^{36,37} Moreover, certain IL structures enhance the immunogenicity of mRNA LNP vaccines, further demonstrating their clinical relevance.^{38,39} With the important roles ILs play in determining the success of LNPs, IL structure is of critical significance when designing new LNPs.

The typical structure of an IL consists of an amine core attached to alkyl tails. IL cores containing piperazine rings have been widely used in RNA LNPs.^{19,38,40,41} The lipid tail of one such core was optimized for siRNA delivery, which identified C12-200 as an ideal IL for hepatic delivery of siRNA LNPs.^{42–45} C12-200 has also been successfully used to deliver mRNA.^{46–48} In addition to the IL, it has been shown that other lipid components also influence LNP transfection. Different phospholipid structures have been found to be successful for LNP-mediated delivery of siRNA versus mRNA, indicating that the most efficacious IL structures may also vary between cargo types.^{47,49–51} Furthermore, as mRNA molecules exhibit greater size variation than siRNA cargos,^{52,53} it is essential to optimize IL structures specifically for mRNA delivery.

Here, we aim to investigate IL tail length as it relates to mRNA size. We synthesized a library of ILs with alkyl tails of varying lengths

based around C12-200. An LNP library was formulated by altering both the length of the IL tail and the size of the mRNA cargo. It was found that both the IL tail length and mRNA size influenced the efficacy of the LNPs. The C10-200 LNP formulated with luciferase mRNA outperformed the other luciferase LNPs, enhancing transfection compared with the C12-200 LNP 3-fold in vitro and 10-fold in vivo. LNPs formulated with EPO, a smaller mRNA than luciferase mRNA, and Cas9, a larger mRNA, resulted in varying transfection profiles. The C13-200 LNP formulated with EPO mRNA led to in vivo EPO production at levels similar to the C12-200 LNP, and the C9-200 LNP formulated with Cas9 mRNA led to a 3-fold increase in indels compared with the C12-200 LNP. Taken together, our results suggest that ILs with longer tails may be optimal for delivering smaller mRNAs, whereas ILs with shorter tails may be most efficacious for the delivery of larger mRNAs.

2 | MATERIALS AND METHODS

2.1 | Materials

LNP lipid excipients, excluding ILs, were purchased from Avanti Polar Lipids (Alabaster, AL, USA). Cas9, erythropoietin (EPO), and firefly luciferase (FLuc) mRNA were purchased from TriLink Biotechnologies (San Diego, CA, USA) and contained 5-methoxyuridine substitutions. TTR sgRNA, containing the sequence 5'-ususasCAGCCAC GUCUACAGCAGUUUUAGA gcuagaaauagc AAGUUAAAAU AAGGCUAGUC CGUUAUCA acugaaaaagu ggcaccgagu cggugcusususu-3', where capital letters refer to RNA residues, lowercase letters refer to 2'-O methyl residues, and s refers to phosphorothioate backbone modifications, were synthesized by Axolabs (Kulmbach, Germany).

2-hexyloxirane, 2-octyloxirane, 2-decyloxirane, 2-dodecyloxirane, and 2-tetradecyloxirane were purchased from TCI (Montgomeryville, PA, USA). 1-nonene and 1-undecene were purchased from AstaTech (Bristol, PA, USA). N1-(2-(4-(2-aminoethyl)piperazin-1-yl)ethyl)ethane-1,2-diamine (200) was purchased from Enamine (Kyiv, Ukraine). Chloroform-d was purchased from Acros Organics (Geel, Belgium). All solvents were purchased from Fisher Scientific (Waltham, MA, USA). All other chemical reagents were purchased from MilliporeSigma (St. Louis, MO, USA).

2.2 | Synthesis

Flash chromatography was performed on a Teledyne Isco (Lincoln, NE, USA) CombiFlash NextGen 300+ with evaporative light

scattering detection using Redisep Gold[®] silica gel disposable flash columns. Solvent removal was performed using a Büchi (New Castle, DE, USA) Rotavapor[®] R-300 System Professional. ¹H and ¹³C NMR spectra were acquired in chloroform-d on a Bruker (Billerica, MA, USA) Avance Neo 400 MHz spectrometer. Nominal mass accuracy LC-MS data were obtained using a Waters (Milford, MA, USA) Acquity UPLC system equipped with a Waters TUV detector (254 nm) and a Waters SQD single quadrupole mass analyzer with electrospray ionization. An Acquity UPLC HSS C18, 1.7 μ m, 2.1 \times 50 mm column was used with a 2 min wash followed by a gradient mobile phase from 50% water (1% trifluoroacetic acid) and 50% acetonitrile (1% trifluoroacetic acid) to 100% acetonitrile (1% trifluoroacetic acid).

2.2.1 | General procedure “A”: Epoxide synthesis

Epoxide synthesis was conducted by means of alkene epoxidation. To a 100 mL round bottom flask was added the corresponding alkene (1.0 equiv.) and dichloromethane (5 mL). The flask was stirred for 1 min and cooled to 0°C. Then, was added one half of a solution of meta-chloroperoxybenzoic acid (70% pure, 2.0 equiv.) in dichloromethane (25 mL) dropwise. The solution was stirred for 1 h, and the second half of the solution of meta-chloroperoxybenzoic acid in dichloromethane was added dropwise. The reaction flask was stirred at 0°C for 1 h, and then stirred at room temperature for 15 h. The reaction was quenched by adding 30 mL of a 1:1 solution of sat. sodium bicarbonate and sat. sodium thiosulfate. The layers were separated and the organic layer was washed with brine (1 \times 30 mL). The aqueous layers were combined and extracted with DCM (3 \times 15 mL). The organic layers were combined, dried with magnesium sulfate, filtered, and concentrated in vacuo. The compound was further purified by flash chromatography using a CombiFlash with a liquid injection into a 24 g column. The mobile phase consisted of a gradient of 100% hexanes to 90% hexanes and 10% ethyl acetate over 18 min using a flow rate of 35 mL/min. The products were isolated as clear oils and characterized using ¹H NMR and ¹³C NMR. Specific conditions for each reaction and corresponding spectra can be found in the Data S1.

2.2.2 | General procedure “B”: IL synthesis

IL synthesis was conducted according to a procedure modified from Love et al.⁵⁴ To a 1 dram vial was added the polyamine core 200 (1.0 equiv.), the corresponding epoxide (6.0 equiv.), and ethanol (0.3 mL). The reaction was stirred at 80°C for 48 h. The crude product was diluted with dichloromethane (0.7 mL) and purified by flash chromatography using a CombiFlash with a liquid injection into a 4 g column. The mobile phase consisted of a gradient of 95% dichloromethane and 5% Ultra solution (75% dichloromethane, 22% methanol, and 3% aqueous ammonium hydroxide by volume) to 80% dichloromethane and 20% Ultra solution over 35 min with a flow rate of 7 mL/min. The products were isolated as viscous oils and characterized using ¹H

NMR and LC-MS. Specific conditions for each reaction and corresponding spectra can be found in Data S1.

2.3 | IL hydrophobicity calculations

Computational studies were carried out to evaluate the physicochemical properties for each IL. The octanol-water partition coefficient (ALogP) was calculated using the Ghose and Crippen's method.^{55,56} The distribution coefficient (LogD) under pH = 7.4 was calculated using the pK_a of each IL using the method described by Tielker et al.⁵⁷

2.4 | LNP formulation

The organic phase was prepared by dissolving the corresponding IL, 18:1 Δ 9-Cis phosphoethanolamine (DOPE), cholesterol, and 14:0 PEG2000 phosphoethanolamine (C14-PEG2000) in ethanol at a molar ratio of 35:16:46.5:2.5, respectively. The organic phase for LNP accumulation experiments additionally contained DiR (5 mol %). The aqueous phase was prepared by dissolving the corresponding mRNA in 10 mM citrate buffer at pH 3 (Teknova, Hollister, CA, USA). The IL to mRNA weight ratio for all LNPs was 10:1.⁵⁰ The two phases were loaded into separate glass syringes (Hamilton Company, Reno, NV) and LNPs were formed by chaotic mixing of the organic and aqueous phases at a 1:3 volume ratio in a microfluidic device using a Pump 33 DDS syringe pump (Harvard Apparatus, Holliston, MA, USA).⁵⁸ The LNPs were subsequently dialyzed against 1X PBS (Thermo Fisher Scientific, Waltham, MA, USA) in 20 kDa molecular weight cutoff dialysis cassettes (Thermo Fisher Scientific) for 2 h and sterile filtered through 0.22 μ m syringe filters (Genesee Scientific, El Cajon, CA). LNPs were stored at 4°C.

2.5 | LNP characterization

Encapsulated mRNA concentration and encapsulation efficiency of the LNPs were measured using a Quant-iT RiboGreen assay (Thermo Fisher Scientific) as previously described.^{59,60} Each LNP was diluted 100-fold in two microcentrifuge tubes containing either 1X tris-EDTA (TE) buffer or 1% (v/v) Triton X-100 (Alfa Aesar, Haverhill, MA, USA) in 1X TE buffer. The Triton X-100 samples were mixed thoroughly and allowed to incubate for 5 min to achieve lysis of LNPs. LNPs in 1X TE buffer, LNPs in 1% Triton X-100 buffer, and mRNA standards were placed in quadruplicate in black-walled 96-well plates. RiboGreen detection reagent was added to each well per manufacturer instructions. The plate was shaken on a plate reader in the dark at 200 rpm for 5 min, and then fluorescence intensity was read on an Infinite 200 Pro plate reader (Tecan, Morrisville, NC, USA) at an excitation wavelength of 480 nm and an emission wavelength of 520 nm. Encapsulated mRNA concentration was estimated using a standard curve estimated from a univariate least squared linear regression. Encapsulation efficiency was calculated as $EE = 1 - \frac{R_{TE}}{R_{TX}}$, where R_{TE} is

the measured free RNA content in TE buffer, and R_{TX} is the measured total RNA content in 0.1% Triton X-100 buffer. Encapsulation efficiencies were reported as mean \pm standard deviation ($n = 4$ technical replicates).

The hydrodynamic diameter and polydispersity index (PDI) of each LNP were measured using a DynaPro Plate Reader III (Wyatt Technology, Santa Barbara, CA, USA). Each LNP was diluted 10-fold in 1X PBS and placed in a 384-well Aurora plate (Wyatt Technology). The plate was centrifuged at 400 g for 5 min and then loaded onto the plate reader. Hydrodynamic diameter was reported as mean \pm standard deviation, where standard deviation was calculated as $STD = \sqrt{PDI} \times \text{diameter}$ ($n = 3$ technical replicates).

The surface ζ -potential of each LNP was measured using a Zetasizer Nano (Malvern Instruments, Malvern, UK). Each LNP was diluted 100-fold in deionized water (Thermo Fisher Scientific) and placed into a disposable folded capillary cell (Malvern Instruments) before measurements were collected by the instrument. ζ -potential was reported as mean \pm standard deviation ($n = 3$ technical replicates).

2.6 | In vitro studies

Hep G2 cells were purchased from ATCC (cat. HB-8065, Manassas, VA, USA) and maintained in Dulbecco's modified Eagle medium with L-glutamine (DMEM; Gibco, Dublin, Ireland) supplemented with 10% (v/v) fetal bovine serum (Gibco) and 1% (v/v) penicillin-streptomycin (Gibco) at 37°C in a humidified incubator with 5% CO₂. Cells were diluted 1:1 in 0.4% Trypan Blue Stain (Thermo Fisher Scientific) and counted using a Countess 3 Automated Cell Counter (Thermo Fisher Scientific).

Cells were plated at 20,000 cells per well in 100 μ L of DMEM and left to adhere for 24 h. The media were removed and the cells were treated with a solution of LNPs formulated with FLuc mRNA in DMEM at a dose of 20 ng of mRNA per 20,000 cells to evaluate the in vitro luciferase expression mediated by each LNP. DMEM alone was used as a negative control, and LNPs formulated with C12-200 were used as a positive control. The LNP-treated cells incubated at 37°C for 24 h. Media were removed and 50 μ L of 1X reporter lysis buffer (Promega, Madison, WI, USA) was added to each well, followed by 100 μ L of luciferase assay substrate (Promega). The plate was shook on a plate reader in the dark at 200 rpm for 10 min, and an Infinite 200 Pro plate reader (Tecan) was used to quantify luminescence intensity. Luminescence intensity was normalized by dividing the luminescence of each well by the average luminescence intensity of the wells treated with C12-200. Normalized luciferase expression was reported as mean \pm standard deviation ($n = 3$ biological replicates; each averaged from $n = 4$ technical replicates).

The cytotoxicity of the LNPs was measured using the same plating and treatment methods as described above. After 24 h of incubating the LNP-treated cells at 37°C, 100 μ L of CellTiter-Glo (Promega) was added to each well. The plate was shook on a plate reader in the dark at 200 rpm for 10 min, and an Infinite 200 Pro plate reader (Tecan) was used to quantify luminescence intensity. Luminescence

intensity was normalized by dividing the luminescence of each well by the average luminescence intensity of the untreated wells. Percent cell viability was reported as mean \pm standard deviation ($n = 3$ biological replicates; each averaged from $n = 4$ technical replicates).

2.7 | In vivo studies

All animal use was in accordance with the guidelines and approval from the University of Pennsylvania's Institutional Animal Care and Use Committee (IACUC; protocol #806540). BALB/cJ (*Mus musculus*) female mice (6–8 weeks old, approximately 20 g average weight) were purchased from Jackson Laboratory (Bar Harbor, ME, USA).

Mice were injected with LNPs formulated with FLuc mRNA at a dose of 0.1 mg of mRNA per kg of body mass (mg/kg) via the lateral tail vein. A solution of *D*-luciferin (Biotium, Fremont, CA, USA) in 1X PBS was prepared at a concentration of 15 mg/mL. After 6 h, the mice were injected intraperitoneally with the *D*-luciferin solution (0.2 mL, 15 mg/mL). After 5 min, the mice were euthanized with CO₂ and the heart, lungs, liver, kidneys, and spleen were removed and imaged using an in vivo imaging system (IVIS; PerkinElmer, Waltham, MA, USA). Luminescence flux was quantified with the Living Image Software (PerkinElmer). For LNP accumulation experiments, fluorescence was quantified with the Living Image Software at an excitation/emission of 750/780 nm. Rectangular regions of interest (ROI) of constant size were placed around the corresponding images of each organ. Total luminescence flux was reported as mean \pm standard deviation ($n = 3$ biological replicates). Total radiant efficiency was reported as mean \pm standard deviation ($n = 3$ biological replicates).

Mice were injected with LNPs formulated with EPO mRNA at a dose of 0.1 mg/kg via the lateral tail vein. After 6 h, blood was collected from the mice via retro-orbital bleeding as described by Jiang et al.⁶¹ Blood collection was repeated at 30 h using the same procedure. Serum was isolated by centrifuging the blood samples in Microtainer blood collection tubes containing serum separatory gel (BD, Franklin Lakes, NJ, USA) for 10 min at 3500 rpm. Serum EPO levels were measured using a human erythropoietin ELISA kit (Abcam, Cambridge, UK) according to manufacturer instructions. Plasma EPO level was reported as mean \pm standard deviation ($n = 3$ biological replicates).

Mice were injected with LNPs formulated with Cas9 mRNA and TTR sgRNA at a 4:1 mass ratio at a dose of 0.5 mg/kg via the lateral tail vein. After 7 days, the mice were euthanized with CO₂ and livers were collected for indel analysis. DNA was extracted from each liver using a DNeasy Blood & Tissue Kit (Qiagen, Hilden, Germany) and quantified using a nanodrop plate attachment on an Infinite 200 Pro plate reader (Tecan). Polymerase chain reaction (PCR) amplification of the TTR target site was carried out using Q5 High-Fidelity DNA Polymerase (New England Biolabs, Ipswich, MA, USA) and the primer sequences mTTR-exon2-F, 5'-CGGTTTACTCTGACCCATTTC-3' and mTTR-exon2-R, 5'-GGGCTTCTACAAGCTTACC-3'. Deep sequencing of the TTR amplicons and determination of the on-target indel frequency was performed according to a procedure modified from Wang

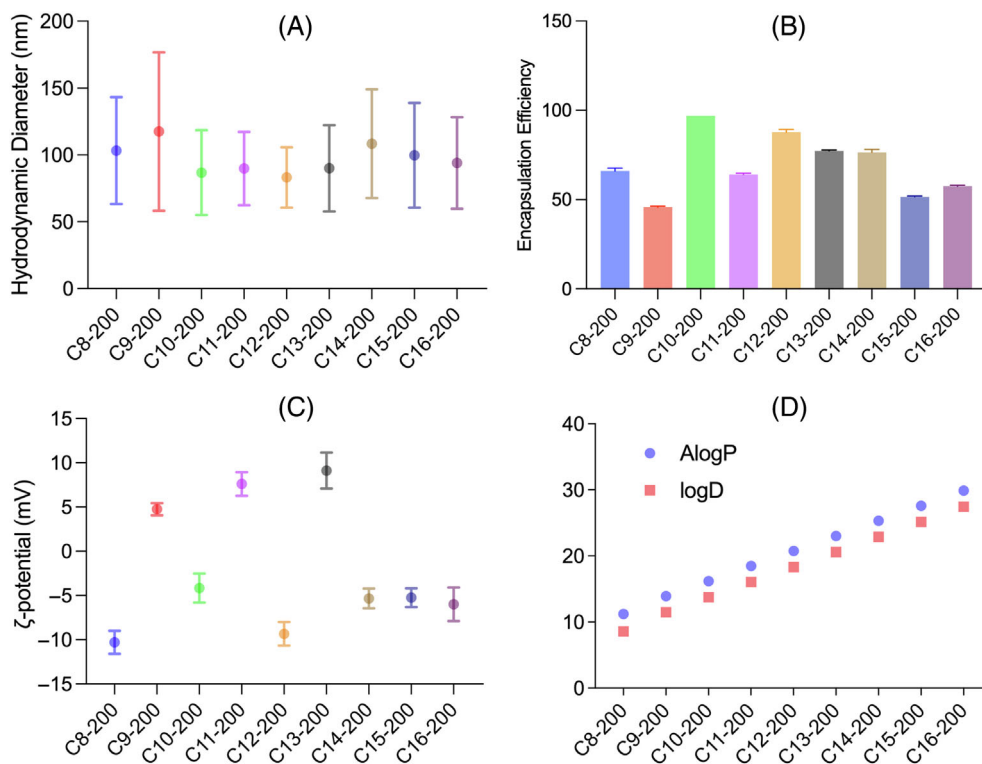


FIGURE 2 Characterization of each ionizable lipid (IL) and the corresponding lipid nanoparticles (LNP) formulated with FLuc mRNA. (A) Hydrodynamic diameter of each LNP, reported as mean \pm standard deviation where standard deviation was calculated as $STD = \sqrt{PDI} \times \text{diameter}$ ($n = 3$ technical replicates). (B) Encapsulation efficiency of each LNP, reported as mean \pm standard deviation ($n = 4$ technical replicates). (C) ζ -potential of each LNP, reported as mean \pm standard deviation ($n = 3$ technical replicates). (D) Octanol-water partition coefficient (AlogP) and distribution coefficient under pH = 7.4 (logD) of each IL.

LNPs had encapsulation efficiencies below 70%. As IL structure was the only variable changing between LNP formulations, the hydrophobicity of each IL was also quantified (Figure 2D). As expected, the calculations for AlogP and logD demonstrated increasing IL hydrophobicity with increasing alkyl tail length. Interestingly, changes in IL hydrophobicity between LNP formulations did not mirror the observed changes in encapsulation efficiency. Additionally, both LNP size and ζ -potential remained consistent with varying IL hydrophobicity, suggesting that IL hydrophobicity does not alter LNP physical properties appreciably for ILs containing the 200 core.

3.3 | LNP-mediated luciferase mRNA delivery in vitro and in vivo

LNPs formulated with luciferase (FLuc) mRNA, a moderately sized mRNA that contains 1929 base pairs, were evaluated in both in vitro and in vivo models. The efficacy of LNP-mediated FLuc mRNA transfection was evaluated in an in vitro HepG2 cell model. Cells were treated with LNPs at a dose of 20 ng of mRNA per 20,000 cells and incubated for 24 h. The relative luminescence expression results indicated that LNPs formulated with ILs of varying tail lengths enhanced transfection. Particularly, the C10-200, C13-200, and C16-200 LNPs exhibited a significant increase in transfection compared with the C12-200 control LNP (Figure 3A). When examined for cytotoxicity, none of the formulations exhibited statistically significant changes in cell viability compared with the untreated negative control formulation or the C12-200 positive control LNP (Figure 3B). To evaluate mRNA LNP transfection in vivo, LNPs were administered intravenously into BALB/cJ mice at a dose of 0.1 mg/kg. After 6 h, the mice

were euthanized and the organs were imaged to evaluate luminescence (Figure 3C–E). Similar to the in vitro results, the C10-200 LNP exhibited a 10-fold increase in liver transfection compared with the C12-200 control LNP; however, in contrast to the in vitro results, the C13-200 and C16-200 LNPs did not enhance luminescence flux relative to the C12-200 LNP (Figure 3D). Additionally, the C9-200, C11-200, and C13-200 LNPs induced similar luciferase expression in the liver compared with the C12-200 LNP. The C8-200, C14-200, and C16-200 LNPs had reduced liver luciferase expression compared with the C12-200 LNP. Interestingly, the C15-200 LNP did not enhance liver transfection relative to the PBS negative control. To test whether the increases in luminescence were due to enhanced LNP accumulation, the C10-200 and C12-200 LNPs were reformulated with DiR and administered intravenously into BALB/cJ mice at a dose of 0.1 mg/kg. No difference in total radiant efficiency was found, indicating similar liver accumulation for both LNPs. Equal LNP accumulation in the spleen was also observed, but this was hypothesized to be due to vasculature and fenestration in the spleen as spleen luminescence was not observed with either LNP. Since increased translation and similar accumulation were observed in the liver, it was hypothesized that the variations in translation are due to differences in endosomal escape between the two LNPs.^{25,26}

3.4 | In vivo LNP-mediated delivery of functional mRNA

LNPs formulated with either EPO or Cas9 mRNA, two functional mRNAs, were evaluated in vivo. EPO is a glycoprotein hormone produced by the peritubular cells of the kidney to stimulate red blood cell

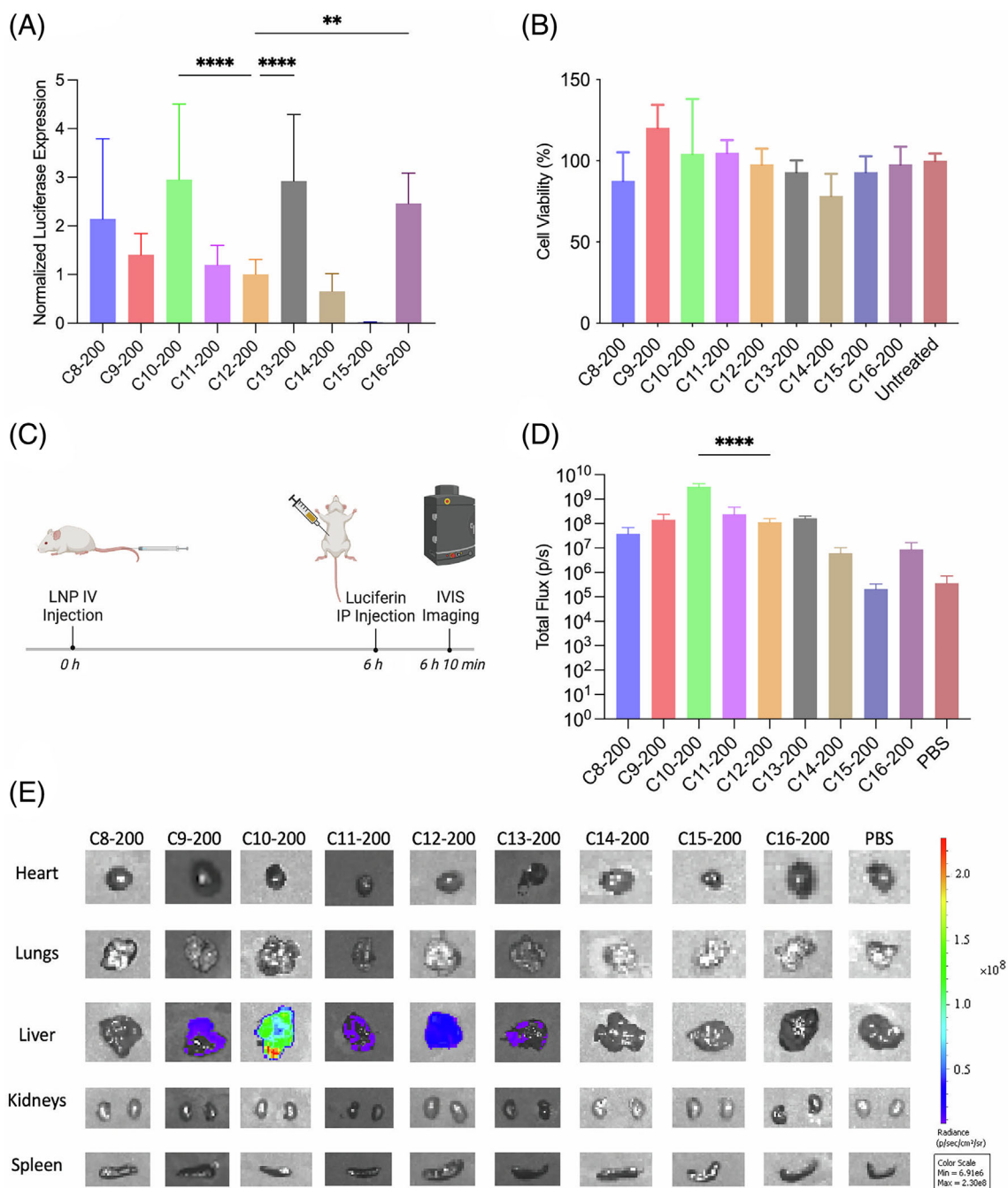


FIGURE 3 In vitro and in vivo luciferase mRNA lipid nanoparticle (LNP) studies demonstrate higher transfection of C10-200 LNP compared with C12-200 LNP. (A, B) Hep G2 cells were treated with LNPs at a dose of 20 ng of FLuc mRNA per 20,000 cells for 24 h. Luciferase expression of each treatment group was normalized to the C12-200 group. Luciferase expression (A) is reported as mean ± standard deviation ($n = 3$ biological replicates; each averaged from $n = 4$ technical replicates). Percent cell viability (B) for each treatment group was normalized to the untreated group and is reported as mean ± standard deviation ($n = 3$ biological replicates; each averaged from $n = 4$ technical replicates). One-way ANOVAs with post hoc Student's t -tests using the Holm-Šidák correction for multiple comparisons were used to compare normalized luciferase expression and percent cell viability across treatment groups. No statistically significant comparisons were found to the untreated group in the viability study. (C) In vivo FLuc mRNA LNP experiment schedule. (D) Quantification of FLuc mRNA LNP delivery (0.1 mg/kg) to the liver. One-way ANOVAs with post hoc Student's t -tests using the Holm-Šidák correction for multiple comparisons were used to compare relative luminescence flux across treatment groups. Data are reported as mean ± standard deviation ($n = 3$ biological replicates). (E) In vivo imaging system (IVIS) images of luciferase mRNA LNP delivery to the heart, lungs, liver, kidneys, and spleen. For each treatment group, representative IVIS images of each organ are shown from the mouse with the liver flux value closest to the mean. * $p \leq 0.05$, ** $p \leq 0.01$, *** $p \leq 0.001$, **** $p \leq 0.0001$.

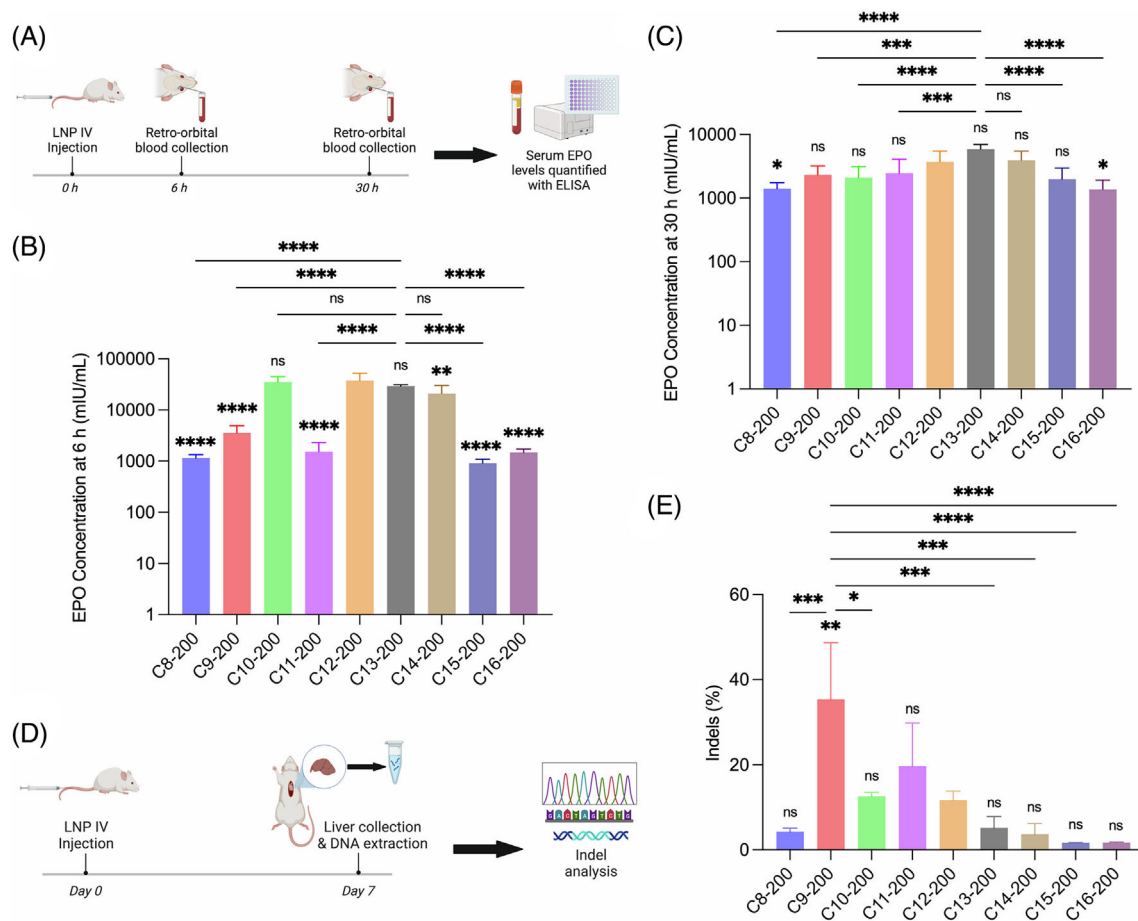


FIGURE 4 In vivo erythropoietin (EPO) and Cas9 mRNA lipid nanoparticles (LNP) studies demonstrate increased EPO transfection with longer ionizable lipid (IL) tail lengths, and increased Cas9 transfection with shorter IL tail lengths. (A) In vivo EPO mRNA LNP experiment schedule. (B, C) EPO serum concentration at 6 h (B) and 30 h (C) following EPO mRNA LNP injection (0.1 mg/kg). One-way ANOVAs with post hoc Student's *t*-tests using the Holm-Šidák correction for multiple comparisons were used to compare EPO serum concentration across treatment groups. Data are reported as mean \pm standard deviation ($n = 3$ biological replicates). Statistical annotations displayed without brackets represent comparisons with the C12-200 treatment group, and statistical annotations displayed with brackets represent comparisons with the C13-200 treatment group. (D) In vivo Cas9 mRNA LNP experiment schedule. (E) Percent indels following Cas9 mRNA LNP injection (0.5 mg/kg). One-way ANOVAs with post hoc Student's *t*-tests using the Holm-Šidák correction for multiple comparisons were used to compare indels across treatment groups. Data are reported as mean \pm standard deviation ($n = 3$ biological replicates). Statistical annotations displayed without brackets represent comparisons with the C12-200 treatment group, and statistical annotations displayed with brackets represent all significant findings in comparison with the C9-200 treatment group. * $p \leq 0.05$, ** $p \leq 0.01$, *** $p \leq 0.001$, **** $p \leq 0.0001$.

production and has been used as a therapeutic for chronic kidney failure.^{65,66} EPO mRNA contains 858 base pairs and is thus smaller than FLuc mRNA. Cas9 mRNA can be used alongside a single-guide RNA to enable in vivo genome editing and is a larger mRNA that contains 4521 base pairs.^{67,68} Here, we evaluated LNPs formulated with Cas9 mRNA and a single guide RNA (sgRNA) targeting transthyretin (TTR). In clinical cases of transthyretin amyloidosis, faulty TTR proteins produced by the liver can accumulate into fibril proteins and lead to heart failure. While previous siRNA LNP therapies, including ONPATRO[®], have required multiple doses to silence TTR translation, the gene editing approach here only requires a single dose to permanently reduce TTR levels.

To evaluate the efficacy of LNP-mediated EPO mRNA delivery, LNPs were administered intravenously into BALB/cJ mice at a dose of

0.1 mg/kg and blood was collected via retro-orbital bleeding for analysis of EPO serum levels at 6 h, when peak IV concentration has been observed, and 30 h, due to an interest in examining the kinetics of EPO mRNA expression (Figure 4A).⁶⁹ At 6 h, the C9-200 and C13-200 LNPs induced EPO production similar to the C12-200 LNP, and the C13-200 LNP induced greater EPO production than all LNPs other than C9-200 and C14-200 (Figure 4B). At 30 h, the C13-200 LNP induced EPO production as well as C12-200, and enhanced EPO serum levels compared with C9-200 (Figure 4C). Similar to the 6 h time point, no difference was found between EPO serum levels in mice treated with the C13-200 and C14-200 LNPs at 30 h. Additionally, both the C12-200 and C13-200 LNPs demonstrated a 10-fold decrease in induced EPO production between 6 h and 30 h, consistent with other findings that mRNA concentration following IV

delivery begins to level out after the initial 6 h peak.⁶⁹ Interestingly, there was no difference found in induced EPO levels between mice treated with the C10-200 and C12-200 LNPs at either timepoint, in contrast to the increased luciferase transfection induced by the C10-200 LNP.

LNPs formulated with Cas9 were administered intravenously into BALB/cJ mice at a dose of 0.5 mg/kg and mouse livers were collected at day 7 post-injection for indel analysis using next-generation sequencing (NGS) (Figure 4D). Similar to the EPO study, no difference was found in indel editing between the C10-200 and C12-200 LNPs (Figure 4E). Notably, the C9-200 LNP induced 35% indels, whereas the C12-200 LNP only induced 10% indels. Treatment with the C9-200 LNP led to greater indels than all formulations other than the C11-200 LNP. The C12-200 LNP displayed only minor increases in indels compared with the C8-200, C13-200, and C14-200 LNPs, which each induced around 5% indels. The C15-200 and C16-200 LNPs both led to less than 2% indels, indicating low transfection. Taken together, these results demonstrate that the ideal IL tail length for mRNA delivery changes for the three mRNA cargos tested.

4 | DISCUSSION

We synthesized a library of ILs based around the structure of C12-200, which varied in terms of IL tail length. Using a simple one-step synthetic scheme, we were able to generate epoxide tails of varying lengths, and this epoxide synthesis allowed for the inclusion of ILs with odd-numbered tail lengths into the library. Since odd-length epoxides are not commonly available commercially, this synthesis enabled the investigation of a complete range of IL tail lengths, which is not typically performed. LNPs formulated with ILs with odd-numbered tails showed varying levels of efficacy with the three mRNA cargos evaluated in vivo. Interestingly, LNP performance varied among neighboring LNPs in the library which were formulated with ILs containing either one additional or one less carbon in each tail. Both the C9-200 and C11-200 LNPs formulated with EPO mRNA led to a 10-fold decrease in EPO serum levels at 6 h compared with the neighboring C10-200 LNP. In contrast, the C9-200 LNP formulated with Cas9 mRNA induced 35% indels, whereas the neighboring C8-200 and C10-200 LNPs induced 4% and 13% indels, respectively. These results indicate that one-carbon differences in IL tail length can lead to significant changes in mRNA LNP transfection, underscoring the importance of our creation of a library consisting of each unique tail length, both even- and odd-numbered.

Following LNP formulation, FLuc mRNA LNPs were characterized. Hydrodynamic diameter and ζ -potential were found to be consistent across formulations, suggesting that neither LNP size nor surface charge mediates the relationship between IL tail length and LNP efficacy. IL hydrophobicity was quantified using AlogP and logD calculations, which demonstrated increasing IL hydrophobicity with the increasing alkyl tail length. As LNP transfection did not follow a similar trend in any of the three mRNAs evaluated, IL hydrophobicity is likely not a preeminent determinant factor for LNP efficacy. Encapsulation

efficiency varied across FLuc mRNA LNP formulations, but was not correlated with IL hydrophobicity, indicating that hydrophobicity alone did not impact LNP formation. Although encapsulation efficiency varied widely across the LNPs, two FLuc mRNA LNPs with low encapsulation efficiencies, C9-200 and C13-200, still led to similar luciferase transfection compared with the C12-200 LNP in vivo. Given that changing the structure of LNP lipid components can impact the optimal molar formulation ratio, it is possible that individually optimizing the molar ratio for LNPs formulated with each IL could improve LNP formation and encapsulation efficiency.^{50,70,71} This could be achieved through an orthogonal design of experiments as previously demonstrated by our previous work.^{40,70}

LNPs were initially formulated with each IL in the library and FLuc mRNA. FLuc mRNA is one of the most common gene reports used to screen and validate LNP efficacy in vivo due to its low background.^{50,72,73} We found that the C10-200 LNP enhanced liver transfection by over 10-fold compared with the C12-200 LNP. It is significant that decreasing IL alkyl tail length by just two carbons each led to such a large increase in liver delivery compared with a gold-standard IL. Given that C12-200 is commonly used as the IL in FLuc screening experiments, C10-200 could be used in similar studies to increase delivery of FLuc mRNA-encapsulated LNPs to the liver. While LNPs formulated with FLuc mRNA were also evaluated in vitro in a Hep G2 cell model, it was found that the in vitro luciferase expression experiment was only minimally predictive of in vivo LNP transfection. These results indicate that despite using a common liver cell line, it is difficult to accurately predict in vivo LNP behavior in an in vitro model. This discrepancy is consistent with other findings, and is likely due to the many biological factors at play in vivo that cannot be replicated in an in vitro experimental setup. In addition to the change in transfection observed when transitioning from an in vitro to in vivo model, transfection also changed significantly when LNPs were formulated with mRNA cargos of varying sizes. In addition to the moderately-sized FLuc mRNA, we investigated a relatively small mRNA, EPO, and a larger mRNA, Cas9 in vivo. It was found that multiple LNPs formulated with ILs of varying tail lengths performed as well as or better than the C12-200 LNP across all three mRNA sizes tested, and the top performers varied depending on the mRNA cargo used.

Taken together, our findings suggest that shorter IL tails may lead to higher transfection of LNPs encapsulating larger mRNAs, and that longer IL tails may be more efficacious for delivering smaller mRNA cargos. The C9-200 LNP, formulated with an IL containing alkyl tails of 9 carbons each, led to the highest transfection of LNPs formulated with Cas9, the largest mRNA we tested. In contrast, EPO serum levels in mice that were administered the C13-200 LNP were similar to those of mice administered the C12-200 control LNP at both the 6 h and 30 h timepoints post-injection. Here, we demonstrated the significance of IL tail length to LNP transfection for ILs formulated with the polyamine core 200. While this study focused on examining this specific core due to its common use in mRNA LNP applications, the results are limited to LNPs formulated with the polyamine core 200. We hypothesize that IL tail length could play a significant role for

LNPs formulated with other cores and aim to further probe the impacts of adjusting IL tail length in the future using other polyamine cores. While all three of the mRNAs tested are transcribed in the cytoplasm, the varying functions of each mRNA necessitate secretion of the EPO protein from the cell and translocation of the Cas9 protein to the nucleus.^{68,74} To determine whether our findings can be fully attributed to a relationship between IL tail length mRNA size, future studies should investigate additional mRNAs of each size with different functional profiles. Finally, future work should aim to elucidate a mechanistic approach behind our findings.

5 | CONCLUSION

We explored the relationship between IL tail length and LNP efficacy with three mRNA cargos of different sizes. Provided that ILs play an important role in determining LNP efficacy, we aimed to elucidate the influence of IL lipid tail length on LNP-mediated mRNA delivery. We found that LNPs formulated with C10-200, an IL in which each alkyl tail is two carbons shorter than the gold standard IL C12-200, exhibited a 10-fold increase in in vivo liver delivery of luciferase mRNA, a moderately-sized mRNA, compared with the C12-200 control LNP. Furthermore, we found that the relative performance of these two FLuc mRNA LNPs does not translate to LNP-mediated delivery of different mRNA cargos. When formulated with EPO mRNA, a smaller cargo, the C13-200 LNP induced EPO production in vivo at levels similar to the C12-200 LNP. Finally, in vivo evaluation of LNPs formulated with Cas9 mRNA demonstrated that the C9-200 LNP induced over three times the quantity of indels compared with the C12-200 LNP. Our results suggest that mRNA size is a determinant factor for optimizing the alkyl tail length of ILs in LNPs. Future studies should investigate similar IL libraries using different amine cores in an effort to elucidate the mechanism behind the observed changes in LNP efficacy.

ACKNOWLEDGMENTS

M.J.M. acknowledges support from a US National Institutes of Health (NIH) Director's New Innovator Award (no. DP2TR002776), a Burroughs Wellcome Fund Career Award at the Scientific Interface (CASI), the American Cancer Society (RSG-22-122-01-ET), and an NSF CAREER Award (no. CBET-2145491). M.S.P. acknowledges support from the National Institute of Dental & Craniofacial Research (NIDCR) of the NIH under Award Number T90DE030854 and the Center for Innovation & Precision Dentistry (CiPD) at the University of Pennsylvania. E.L.H. acknowledges support from a National Science Foundation (NSF) Graduate Research Fellowship (no. 1845298). R.P. acknowledges support from an NIH NHLBI F30 fellowship (F30HL162465-01A1). The content is solely the responsibility of the authors and does not necessarily represent the official views of the National Institutes of Health. The authors also acknowledge the NSF Major Research Instrumentation Program (award NSF CHE-1827457) and Vagelos Institute for Energy Science and Technology for

supporting the purchase of the NMR used in this study. Figures were created with BioRender.

CONFLICT OF INTEREST STATEMENT

The authors declare no conflicts of interest.

DATA AVAILABILITY STATEMENT

The data that support the findings of this study are available from the corresponding author upon reasonable request.

ORCID

Michael J. Mitchell  <https://orcid.org/0000-0002-3628-2244>

REFERENCES

- Boczkowski D, Nair SK, Gilboa E. Dendritic cells pulsed with RNA are potent antigen-presenting cells in vitro and in vivo. *J Exp Med*. 1996;184:465-472.
- Zhou WZ, Hoon DS, Huang SK, et al. RNA melanoma vaccine: induction of antitumor immunity by human glycoprotein 100 mRNA immunization. *Hum Gene Ther*. 1999;10:2719-2724.
- Koido S, Kashiwaba M, Chen D, Gendler S, Kufe D, Gong J. Induction of antitumor immunity by vaccination of dendritic cells transfected with MUC1 RNA. *J Immunol*. 2000;165:5713-5719.
- Pardi N, Hogan MJ, Porter FW, Weissman D. mRNA vaccines – a new era in vaccinology. *Nat Rev Drug Discov*. 2018;17:261-279.
- Conry RM, LoBuglio A, Wright M, et al. Characterization of a messenger RNA polynucleotide vaccine vector. *Cancer Res*. 1995;55:1397-1400.
- Mandl CW, Aberle JH, Aberle SW, Holzmann H, Allison SL, Heinz FX. In vitro-synthesized infectious RNA as an attenuated live vaccine in a flavivirus model. *Nat Med*. 1998;4:1438-1440.
- Rittig SM, Haentschel M, Weimer KJ, et al. Intradermal vaccinations with RNA coding for TAA generate CD8+ and CD4+ immune responses and induce clinical benefit in vaccinated patients. *Mol Ther*. 2011;19:990-999.
- Qiu P, Ziegelhoffer P, Sun J, Yang S. Gene gun delivery of mRNA in situ results in efficient transgene expression and genetic immunization. *Gene Ther*. 1996;3:262-268.
- Wang J, Exline CM, DeClercq JJ, et al. Homology-driven genome editing in hematopoietic stem and progenitor cells using ZFN mRNA and AAV6 donors. *Nat Biotechnol*. 2015;33:1256-1263.
- Mahiny AJ, Dewerth A, Mays LE, et al. In vivo genome editing using nuclease-encoding mRNA corrects SP-B deficiency. *Nat Biotechnol*. 2015;33:584-586.
- Lorenz C, Fotin-Mlecsek M, Roth G, et al. Protein expression from exogenous mRNA: uptake by receptor-mediated endocytosis and trafficking via the lysosomal pathway. *RNA Bio*. 2011;8:627-636.
- Han X, Mitchell MJ, Guangjun N. Nanomaterials for therapeutic RNA delivery. *Matter*. 2020;3:1948-1975.
- Buschmann MD, Carrasco MJ, Alishetty S, Paige M, Alameh MG, Weissman D. Nanomaterial delivery systems for mRNA vaccines. *Vaccine*. 2021;9:65.
- Mitchell MJ, Billingsley MM, Haley RM, Wechsler ME, Peppas NA, Langer R. Engineering precision nanoparticles for drug delivery. *Nat Rev Drug Discov*. 2021;20:101-124.
- Thanh Le T, Cramer JP, Chen R, Mayhew S. Evolution of the COVID-19 vaccine development landscape. *Nat Rev Drug Discov*. 2020;19:667-668.
- Verbeke R, Lentacker I, De Smedt SC, Dewitte H. The dawn of mRNA vaccines: the COVID-19 case. *J Control Release*. 2021;333:511-520.
- Swingle KL, Hamilton AG, Mitchell MJ. Lipid nanoparticle-mediated delivery of mRNA therapeutics and vaccines. *Trends Mol Med*. 2021;27:616-617.

18. Xucheng H, Zaks T, Langer R, Dong Y. Lipid nanoparticles for mRNA delivery. *Nat. Rev. Mater.* 2021;6:1078-1094.
19. Han X, Zhang H, Butowska K, et al. An ionizable lipid toolbox for RNA delivery. *Nat Commun.* 2021;12:7233.
20. Carrasco MJ, Alishetty S, Alameh MG, et al. Ionization and structural properties of mRNA lipid nanoparticles influence expression in intramuscular and intravascular administration. *Commun Biol.* 2021;4:956.
21. Kon E, Elia U, Peer D. Principles for designing an optimal mRNA lipid nanoparticle vaccine. *Curr Opin Biotechnol.* 2022;73:329-336.
22. Kulkarni JA, Darjuan MM, Mercer JE, et al. On the formation and morphology of lipid nanoparticles containing ionizable cationic lipids and siRNA. *ACS Nano.* 2018;12:4787-4795.
23. Zhang D, Atochina-Vasserman EN, Lu J, et al. The unexpected importance of the primary structure of the hydrophobic part of one-component ionizable amphiphilic Janus dendrimers in targeted mRNA delivery activity. *J Am Chem Soc.* 2022;144:4746-4753.
24. Semple SC, Akinc A, Chen J, et al. Rational design of cationic lipids for siRNA delivery. *Nat Biotechnol.* 2010;28:172-176.
25. Varkouhi AK, Scholte M, Strom G, Haisma HF. Endosomal escape pathways for delivery of biologicals. *J Control Release.* 2011;151:220-228.
26. Gilleron J, Querbes W, Zeigerer A, et al. Image-based analysis of lipid nanoparticle-mediated siRNA delivery, intracellular trafficking and endosomal escape. *Nature Biotechnol.* 2013;31:638-646.
27. Gujrati M, Malamas A, Shin T, Jin E, Sun Y, Lu ZR. Multifunctional cationic lipid-based nanoparticles facilitate endosomal escape and reduction-triggered cytosolic siRNA release. *Mol Pharm.* 2014;11:2734-2744.
28. Sabnis S, Kumarasinghe ES, Salerno T, et al. A novel amino lipid series for mRNA delivery: improved endosomal escape and sustained pharmacology and safety in non-human primates. *Mol Ther.* 2018;26:1509-1519.
29. Bashiri G, Padilla MS, Swingle KL, Shepherd SJ, Mitchell MJ, Wang K. Nanoparticle protein corona: from structure and function to therapeutic targeting. *Lab Chip.* 2023;23:1432-1466.
30. Aliakbarinodehi N, Gallud A, Mapar M, et al. Interaction kinetics of individual mRNA-containing lipid nanoparticles with an endosomal membrane mimic: dependence on pH, protein corona formation, and lipoprotein depletion. *ACS Nano.* 2022;16:20163-20173.
31. Amici A, Caracciolo G, Digiacomio L, et al. In vivo protein corona patterns of lipid nanoparticles. *RSC Adv.* 2017;7:1137-1145.
32. Francia V, Schifferers RM, Cullis PR, Witzigmann D. The biomolecular corona of lipid nanoparticles for gene therapy. *Bioconjug Chem.* 2020;31:2046-2059.
33. Albertsen CH, Kulkarni JA, Witzigmann D, Lind M, Petersson K, Simonsen JB. The role of lipid components in lipid nanoparticles for vaccines and gene therapy. *Adv Drug Deliv Rev.* 2022;188:114416.
34. Kim M, Jeong M, Hur S, et al. Engineered ionizable lipid nanoparticles for targeted delivery of RNA therapeutics into different types of cells in the liver. *Sci Adv.* 2021;7:eabf4398.
35. Miao L, Lin J, Huang Y, et al. Synergistic lipid compositions for albumin receptor mediated delivery of mRNA to the liver. *Nat Commun.* 2020;11:2424.
36. Sayers EJ, Peel SE, Schantz A, et al. Endocytic profiling of cancer cell models reveals critical factors influencing LNP-mediated mRNA delivery and protein expression. *Mol Ther.* 2019;27:1950-1962.
37. Liu S, Cheng Q, Wei T, et al. Membrane-destabilizing ionizable phospholipids for organ-selective mRNA delivery and CRISPR-Cas gene editing. *Nat Mater.* 2021;20:701-710.
38. Han X, Alameh MG, Butowska K, et al. Adjuvant lipidoid-substituted lipid nanoparticles augment the immunogenicity of SARS-CoV-2 mRNA vaccines. *Nat Nanotechnol.* 2023;18:1105-1114.
39. Li B et al. Enhancing the immunogenicity of lipid-nanoparticle mRNA vaccines by adjuvanting the ionizable lipid and the mRNA. *Nat. Biomed. Eng.* 2023.
40. Safford HC, Swingle KL, Geisler HC, et al. Orthogonal design of experiments for engineering of lipid nanoparticles for mRNA delivery to the placenta. *Small.* 2023;3:e2303568.
41. Palanki R, Bose SK, Dave A, et al. Ionizable lipid nanoparticles for therapeutic base editing of congenital brain disease. *ACS Nano.* 2023;17:13594-13610.
42. Leuschner F, Dutta P, Gorbatov R, et al. Therapeutic siRNA silencing in inflammatory monocytes in mice. *Nat Biotechnol.* 2011;29:1005-1010.
43. Novobrantseva TI, Borodovsky A, Wong J, et al. Systemic RNAi-mediated gene silencing in nonhuman primate and rodent myeloid cells. *Mol Ther Nucleic Acids.* 2012;1:e4.
44. Speicher T, Siegenthaler B, Bogorad RL, et al. Knockdown and knock-out of β 1-integrin in hepatocytes impairs liver regeneration through inhibition of growth factor signaling. *Nat Commun.* 2014;5:3862.
45. Whitehead KA, Dorkin JR, Vegas AJ, et al. Degradable lipid nanoparticles with predictable in vivo siRNA delivery activity. *Nat Commun.* 2014;5:4277.
46. Yin H, Song CQ, Dorkin JR, et al. Therapeutic genome editing by combined viral and non-viral delivery of CRISPR system components in vivo. *Nat Biotechnol.* 2016;34:328-333.
47. Oberli MA, Reichmuth AM, Dorkin JR, et al. Lipid nanoparticle assisted mRNA delivery for potent cancer immunotherapy. *Nano Lett.* 2017;17:1326-1335.
48. Hajj KA. A potent branched-tail lipid nanoparticle enables multiplexed mRNA delivery and gene editing in vivo. *Nano Lett.* 2020;20:5167-5175.
49. Pilkington EH, Suys EJA, Trevaskis NL, et al. From influenza to COVID-19: lipid nanoparticle mRNA vaccines at the frontiers of infectious diseases. *Acta Biomater.* 2021;131:16-40.
50. Kauffman KJ, Dorkin JR, Yang JH, et al. Optimization of lipid nanoparticle formulations for mRNA delivery in vivo with fractional factorial and definitive screening designs. *Nano Lett.* 2015;15:7300-7306.
51. Cheng Q, Wei T, Jia Y, et al. Dendrimer-based lipid nanoparticles deliver therapeutic FAH mRNA to normalize liver function and extend survival in a mouse model of hepatorenal tyrosinemia type I. *Adv Mater.* 2018;30:e1805308.
52. Sommer SS, Cohen JE. The size distributions of proteins, mRNA, and nuclear RNA. *J Mol Evol.* 1980;15:37-57.
53. Schroeder A, Levins CG, Cortez C, Langer R, Anderson DG. Lipid-based nanotherapeutics for siRNA delivery. *J Intern Med.* 2010;267:9-21.
54. Love KT, Mahon KP, Levins CG, et al. Lipid-like materials for low-dose, in vivo gene silencing. *Proc Natl Acad Sci U S A.* 2010;107:1864-1869.
55. Ghose AK, Crippen GM. Atomic physicochemical parameters for three-dimensional structure-directed quantitative structure-activity relationships 1. Partition coefficients as a measure of hydrophobicity. *J Comput Chem.* 1986;7:565-577.
56. Ghose AK, Viswanadhan VN, Wendoloski JJ. Prediction of hydrophobic (lipophilic) properties of small organic molecules using fragmental methods: an analysis of ALOGP and CLOGP methods. *J Phys Chem A.* 1998;102:3762-3772.
57. Tielker N, Tomazic D, Heil J, et al. The SAMPL5 challenge for embedded-cluster integral equation theory: solvation free energies, aqueous pK_a , and cyclohexane-water log D. *J Comput Aided Mol des.* 2016;30:1035-1044.
58. Shepherd SJ, Warzecha CC, Yadavali S, et al. Scalable mRNA and siRNA lipid nanoparticle production using a parallelized microfluidic device. *Nano Lett.* 2021;21:5671-5680.
59. Heyes J, Palmer L, Bremner K, MacLachlan I. Cationic lipid saturation influences intracellular delivery of encapsulated nucleic acids. *J Control Release.* 2005;107:345-366.
60. Swingle KL, Safford HC, Geisler HC, et al. Ionizable lipid nanoparticles for in vivo mRNA delivery to the placenta during pregnancy. *J Am Chem Soc.* 2023;145:4691-4706.

61. Jiang Y, Gaudin A, Zhang J, et al. A “top-down” approach to actuate poly(amine-co-ester) terpolymers for potent and safe mRNA delivery. *Biomaterials*. 2018;176:122-130.
62. Wang L, Smith J, Breton C, et al. Meganuclease targeting of PCSK9 in macaque liver leads to stable reduction in serum cholesterol. *Nat Biotechnol*. 2018;36:717-725.
63. Ramishetti S, Hazan-Halevy I, Palakuri R, et al. A combinatorial library of lipid nanoparticles for RNA delivery to leukocytes. *Adv Mater*. 2020;32:e1906128.
64. Clogston JD, Patri AK. Zeta potential measurement. In: Mcneil SE, ed. *Characterization of Nanoparticles Intended for Drug Delivery*. Methods in Molecular Biology. Vol 697. Humana Press; 2011:63-70.
65. Henry DH, Spivak JL. Clinical use of erythropoietin. *Curr Opin Hematol*. 1995;2:118-124.
66. Macdougall IC, Tucker B, Thompson J, Tomson CRV, Baker LRI, Raine AEG. A randomized controlled study of iron supplementation in patients treated with erythropoietin. *Kidney Int*. 1996;50:1694-1699.
67. Miller JB, Zhang S, Kos P, et al. Non-viral CRISPR/Cas gene editing in vitro and in vivo enabled by synthetic nanoparticle co-delivery of Cas9 mRNA and sgRNA. *Angew Chem Int Ed*. 2017;129:1079-1083.
68. Qiu M, Glass Z, Chen J, et al. Lipid nanoparticle-mediated codelivery of Cas9 mRNA and single-guide RNA achieves liver-specific in vivo genome editing of *Angptl3*. *Proc Natl Acad Sci U S A*. 2021;118:e2020401118.
69. Pardi N, Tuyishime S, Muramatsu H, et al. Expression kinetics of nucleoside-modified mRNA delivered in various nanoparticles to mice by various routes. *J Control Release*. 2015;217:345-351.
70. Billingsley MM, Hamilton AG, Mai D, et al. Orthogonal design of experiments for optimization of lipid nanoparticles for mRNA engineering of CAR T cells. *Nano Lett*. 2022;22:533-542.
71. Swingle KL, Billingsley MM, Bose SK, et al. Amniotic fluid stabilized lipid nanoparticles for in utero intra-amniotic mRNA delivery. *J Control Release*. 2022;341:616-633.
72. El-Mayta R, Padilla MS, Billingsley MM, Han X, Mitchell MJ. Testing the in vitro and in vivo efficiency of mRNA-lipid nanoparticles formulated by microfluidic mixing. *J Vis Exp*. 2023;191:e64810.
73. Guimaraes PPG, Zhang R, Spektor R, et al. Ionizable lipid nanoparticles encapsulating barcoded mRNA for accelerated in vivo delivery screening. *J Control Release*. 2019;316:404-417.
74. Yang T, Li C, Wang X, et al. Efficient hepatic delivery and protein expression enabled by optimized mRNA and ionizable lipid nanoparticle. *Bioact Mater*. 2020;5:1053-1061.

SUPPORTING INFORMATION

Additional supporting information can be found online in the Supporting Information section at the end of this article.

How to cite this article: Mrksich K, Padilla MS, Joseph RA, et al. Influence of ionizable lipid tail length on lipid nanoparticle delivery of mRNA of varying length. *J Biomed Mater Res*. 2024;1-12. doi:[10.1002/jbm.a.37705](https://doi.org/10.1002/jbm.a.37705)